ChemComm

Chemical Communications

rsc.li/chemcomm

ROYAL SOCIETY
OF CHEMISTRY

COMMUNICATION
Stacy M. Copp *et al.*
Heat, pH, and salt: synthesis strategies to favor formation of
near-infrared emissive DNA-stabilized silver nanoclusters

Check for updates

Heat, pH, and salt: synthesis strategies to favor formation of near-infrared emissive DNA-stabilized silver nanoclusters†

Rweetuparna Guha, [iD] [a] Malak Rafik,[a] Anna Gonzàlez-Rosell [iD] [a] and Stacy M. Copp [iD] *[abc]

We present chemical synthesis strategies for DNA-stabilized silver nanoclusters (Ag_N-DNAs) with near-infrared (NIR) emission in the biological tissue transparency windows. Elevated temperatures can significantly increase chemical yield of near-infrared nanoclusters. In most cases, basic pH favors near-infrared nanoclusters while micromolar amounts of NaCl inhibit their formation.

Ag_N-DNAs are promising emitters for biosensing and bioimaging applications.[1,2] These ultrasmall nanoparticles consist of only 10 to 30 silver atoms encapsulated by one to three single-stranded DNA oligomer templates.[3,4] Ag_N-DNAs are reported to exhibit DNA sequence-encoded excitation and emission wavelengths[5,6] as well as high Stokes shifts,[7] quantum yields,[8] and photostabilities.[9–11] The large combinatorial space of DNA sequence has enabled researchers to design a diverse set of Ag_N-DNAs with emission wavelengths ranging from 400 nm to 1200 nm, far into the NIR.[12–17] The sequence-encoded, tunable properties of Ag_N-DNAs and their spectral sensitivity to analytes have led to chemical sensing, biosensing, and imaging applications.[1,2]

We used high-throughput experiments and machine learning to discover thousands of new Ag_N-DNAs.[12–16] This approach enabled successful design of DNA ligand sequences that stabilize Ag_N-DNAs with specific visible and NIR emission colors. NIR-emissive Ag_N-DNAs are of particular interest as novel biocompatible emitters because biological tissues and fluids scatter, absorb, and emit far less light in the tissue transparency windows.[18] Photophysical properties and atomic structures of NIR Ag_N-DNAs discovered in high-throughput

experiments have since been reported.[7,19–26] Mastracco, *et al.* dramatically expanded the space of known NIR-emissive Ag_N-DNAs with over 100 10-base DNA sequences that stabilize Ag_N-DNAs with peak emission > 800 nm.[12] This large data set holds promise for rapid development of NIR Ag_N-DNAs for bioimaging applications in the tissue transparency windows.

This study is motivated by two challenges we identified regarding chemical synthesis of NIR-emissive Ag_N-DNAs. First, we and others have observed that NIR Ag_N-DNAs often take several days to a week after chemical reduction to form in appreciable quantities; in contrast, visibly emissive Ag_N-DNAs typically form within hours and up to one day.[8,19,24] Second, we observe discrepancies between emission spectra of NIR Ag_N-DNAs prepared in microwell plates during high throughput experiments *versus* individually synthesized in single microcentrifuge tubes. Many brightly emissive NIR-emissive Ag_N-DNAs identified in high-throughput experiments form with exceptionally low chemical yield or are even undetectable when prepared in single microcentrifuge tubes. In some cases, formation of visibly emissive Ag_N-DNAs by the same DNA template sequence appears to compete with the NIR-emissive Ag_N-DNA of interest. To advance NIR Ag_N-DNAs for bioimaging applications, this study identifies the causes of discrepancies between microplate synthesis and microcentrifuge tube synthesis, thereby establishing procedures to scale up NIR-emissive Ag_N-DNAs.

We first investigate how synthesis of Ag_N-DNAs differs between microplate and microcentrifuge tube. Robotic liquid handling routines for high-throughput Ag_N-DNA synthesis were designed for good agreement with "by-hand" synthesis of visibly emissive Ag_N-DNAs[12–16] (ESI,† Section 1.2) We observe one key difference between these two methods: Ag_N-DNA samples synthesized in single microcentrifuge tubes are stored at 4 °C immediately after NaBH_4 reduction, except during periodic and brief fluorimetry to assess product formation. Microwell plates are exposed to room temperature for much longer periods after NaBH_4 reduction because fluorimetry of an

[a] Department of Materials Science and Engineering, University of California, Irvine, CA 92697, USA. E-mail: stacy.copp@uci.edu

[b] Department of Physics and Astronomy, University of California, Irvine, CA 92697, USA

[c] Department of Chemical and Biomolecular Engineering, University of California, Irvine, CA 92697, USA

† Electronic supplementary information (ESI) available: Experimental details, full absorbance and emission spectra. See DOI: https://doi.org/10.1039/d3cc02896h

Table 1 Ag$_N$-DNAs with associated peak emission wavelengths, λ_p, and synthesis stoichiometries

Name	DNA sequence (5′ to 3′)	λ_p/nm	[DNA]/µM	[AgNO$_3$]/µM
DNA-1	ACCGCCGGGA	680/820	25	125
DNA-2	CGAACCGGGC	644/820	25	187.5
DNA-3	AGGCGATCAT	580/844	25	187.5
DNA-4	GCCCCCCCGC	670	25	125
DNA-5	CACCCCGAGC	714	20	300
DNA-6	TAGCCCCTGT	562	25	125

Fig. 1 UV-excited emission spectra of Ag$_N$-DNAs prepared at various temperatures and recorded two days after Ag$_N$-DNA synthesis. (a) DNA-**1**, (b) DNA-**2**, (c) DNA-**3**, (d) DNA-**4**, (e) DNA-**5**, and (f) DNA-**6**. Samples were stored at 4 °C (dashed black), 21 °C (dashed red), 4 °C after heating at 37 °C for 4 h (solid black) and at 21 °C after heating at 37 °C for 4 h (solid red). (Fluorimetry was performed on a well plate reader with 850 nm upper spectral range; Fig. S1 (ESI†) shows emission spectra up to 950 nm on a different detector.)

entire 384-microwell plates takes ∼4 hours, and plates are scanned one day and one week after reduction. Moreover, the microwell plate can rise above room temperature in the unrefrigerated plate reader. Thus, we hypothesized that heating above 4 °C favors formation of NIR-emissive Ag$_N$-DNAs.

To test this hypothesis, we investigated how storage temperature after reduction affects Ag$_N$-DNA formation. Six different DNA templates were selected as listed in Table 1, with optimized concentrations of DNA and AgNO$_3$, and the peak emission wavelength(s), λ_p, of emitters produced by these templates. Sequences were chosen from a library of 10-base DNA oligomers designed using machine learning. Selection for this study is based on formation of far-red to NIR products in high-throughput experiments.[12–16]

Ag$_N$-DNAs were synthesized as detailed in ESI.† First, AgNO$_3$ is mixed with an aqueous solution of DNA template in 10 mM NH$_4$OAc at pH 7, room temperature (21 °C); studies show that this forms Ag$^+$–DNA complexes.[27–29] Second, the sample is incubated at 21 °C for 15 minutes. Third, Ag$^+$–DNA complexes are reduced by freshly prepared NaBH$_4$ solution at 0.5 molar ratio to AgNO$_3$ at 21 °C. Finally, solutions are stored in the dark at four distinct conditions until measurement two days later: (1) 4 °C, the "standard" method used for single tube synthesis, (2) 37 °C for 4 hours followed by storage at 4 °C, (3) 21 °C, and (4) 37 °C for 4 hours followed by storage at 21 °C. 37 °C was chosen because well plates are warm to the touch after a 4 hour scan and because thermal stability of Ag$_N$-DNAs at 37 °C is relevant for *in vivo* applications. Heating above 40 °C was avoided due to past evidence of irreversible conversion to larger silver nanoparticles above 40 °C.[8]

Fig. 1 compares Ag$_N$-DNA emission spectra for the four storage conditions above. When stored only at 4 °C, DNA-**1** forms a single dominant product with emission peak λ_p = 680 nm, but when stored at 21 °C and 37 °C for various times, a new Ag$_N$-DNA species with λ_p = 820 nm forms (Fig. 1a). Similarly, DNA-**2** displays a single λ_p = 644 nm peak when stored at 4 °C, but a new NIR-emissive Ag$_N$-DNA (λ_p = 820 nm) forms at higher temperatures (Fig. 1b). For both DNA-**1** and DNA-**2**, NIR peak intensity is greatest when temperature is highest: 37 °C for 4 hours followed by storage at 21 °C for 44 hours. For both DNA-**3** (λ_p = 844 nm) and DNA-**4** (λ_p = 670 nm), emission intensity of the far-red and NIR peaks exhibit *ca.* two- and three-fold increases, respectively, with increased temperature (Fig. 1c and d). For DNA-**3**, this increase accompanies a decrease in a minor λ_p = 580 nm peak, suggesting that a smaller Ag$_N$-DNA product preferentially forms at lower temperatures.

These results support that increased post-reduction storage temperature enhances chemical yield of far-red to NIR-emissive Ag$_N$-DNAs, even forming new NIR Ag$_N$-DNA species that are not detectable at 4 °C. Increased temperature also significantly shortens the days- to week-long incubation times for NIR Ag$_N$-DNA formation.[8,19,24]

Elevated temperature does not increase chemical yield of all far-red or NIR Ag$_N$-DNAs. Increased temperature causes negligible increase in brightness for DNA-**5** (Fig. 1e). For DNA-**6**, both emissive species decreased in brightness with increased temperature (Fig. 1f). Thus, the optimum storage temperature varies among Ag$_N$-DNA species and should be tuned to optimize yield of a specific Ag$_N$-DNA, just as DNA and AgNO$_3$ concentrations are optimized.

Others have reported temperature effects on Ag$_N$-DNA synthesis. Swasey, *et al.* reported heating a red-emissive Ag$_N$-DNA at 40 °C to improve chemical yield,[30] and Petty, *et al.* reported that temperature influenced absorption, excitation, and emission spectra of a NIR-emissive Ag$_N$-DNA by ∼20 nm.[25] We note that Vosch, *et al.* have measured temperature-dependent emission spectra of compositionally pure Ag$_N$-DNAs,[8,31] while here all spectra are collected at room temperature after heating.

The NIR-emissive Ag$_N$-DNA formed by DNA-**3** has molecular formula (DNA)$_2$[Ag$_{20}$]$^{12+}$.[4] We used high performance liquid chromatography (HPLC) and electrospray ionization mass spectrometry (ESI-MS) (Table S3, ESI†) to show that the λ_p = 670 nm species stabilized by DNA-**4** is (DNA)$_2$[Ag$_{14}$]$^{8+}$ (Fig. S13, ESI†). ESI-MS supports that DNA-**6** stabilizes a λ_p = 562 nm (DNA)$_2$[Ag$_{12}$]$^{8+}$ and a NIR-emissive (DNA)$_2$[Ag$_{15}$]$^{9+}$ (Fig. S14, ESI†). These findings agree with reports of how Ag$_N$-DNA electron count correlates with fluorescence spectra.[32] Detailed analysis of all emitters is beyond the scope of this study.
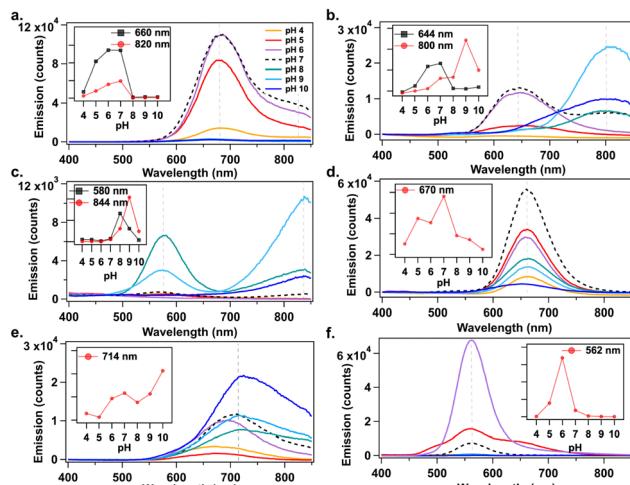
Fig. 2 Changes in emission intensities of (a) DNA-**1**, (b) DNA-**2**, (c) DNA-**3**, (d) DNA-**4**, (e) DNA-**5**, and (f) DNA-**6** when prepared at pH 4 (yellow), 5 (red), 6 (purple), 7 (dashed black), 8 (teal), 9 (light blue), and 10 (dark blue). Insets show change in emission intensity at a specific wavelength (indicated by dashed vertical grey line in the main graph) as a function of pH. Emission spectra recorded two days after NaBH$_4$ reduction.
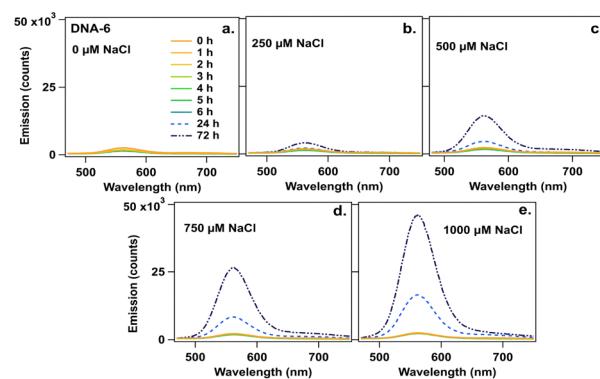
Studies show that pK_a values of deprotonable nucleobases vary over a range of 2 ΔpK_a from 15 to 55 °C.[33] Lee, *et al.*, reported sensing of adenosine 5′-triphosphate (ATP) using pH-dependent change in emission spectra of Ag$_N$-DNAs.[34] The temperature dependence of nucleobase pK_a motivated us to investigate how solution pH affects Ag$_N$-DNA formation. Ag$_N$-DNAs were synthesized in 10 mM NH$_4$OAc solutions from pH 4 to 10. UV-excited emission spectra were recorded after 2 days of storage at 4 °C (ESI†). Fig. 2 shows that Ag$_N$-DNAs with visible emission peaks are brighter at acidic to neutral pH, whereas basic pH favors NIR Ag$_N$-DNAs in most cases. For example, products formed by DNA-**6** (λ_p = 562 nm) are 6-fold brighter at pH 6 compared to pH 7 (Fig. 2f). Similarly, visibly emissive products associated with DNA-**1** (λ_p = 680 nm), DNA-**2** (λ_p = 644 nm), and DNA-**4** (λ_p = 670 nm) are brightest at pH 7 (Fig. 2a, b and d). Preparation at basic pH can significantly increase the brightness of NIR-emissive Ag$_N$-DNAs. For DNA-**2** (λ_p = 644 nm at pH 7), the NIR emissive species (λ_p = 800 nm) increases gradually for pH > 7 (Fig. 2b). DNA-**4** strongly favors formation of the λ_p = 820 nm species at pH 9 (Fig. 2c). DNA-**5** red-shifts and increases in emission intensity at basic pH (Fig. 2e). (Note that peak wavelengths of the NIR species for DNA-**2** differ in Fig. 1b and 2b; purification and mass spectral analysis are needed to confirm if the same NIR species forms at basic pH *versus* elevated temperature.) Thus, solution pH could be used to dramatically increase synthesis yield of far-red and NIR-emissive Ag$_N$-DNAs. Earlier studies by Vosch, *et al.* showed that photophysical properties of Ag$_N$-DNAs stabilized by a cytosine-rich DNA oligomer are unaffected by changes in pH and ionic strength,[35] suggesting that pH does not always affect Ag$_N$-DNA formation. Further studies are required to fully understand how higher pH favors NIR Ag$_N$-DNAs.

Finally, we investigated effects of NaCl on Ag$_N$-DNA emission spectra because residual reagents from commercial nucleic

acid synthesis can cause variability in batch-to-batch Ag$_N$-DNA synthesis. Chlorido ligands were recently reported on Ag$_N$-DNAs, a (DNA)$_2$[Ag$_{16}$Cl$_2$]$^{8+}$ and (DNA)$_2$[Ag$_{15}$Cl]$^{8+}$, even though no chloride source was added during Ag$_N$-DNA synthesis.[24] This finding supports that residual reagents from solid-phase synthesis can significantly affect Ag$_N$-DNA product formation and may cause discrepancy between high-throughput and single-tube Ag$_N$-DNA synthesis. To investigate how residual chloride influences Ag$_N$-DNA formation, the six species in Table 1 were synthesized at their optimal storage temperature at pH 7 (Table S2, ESI†). Two days later, NaCl was added at final concentrations of 250 μM to 1000 μM (∼10 to ∼100-fold excess of chloride per nanocluster). Emission spectra were measured 1 to 6 h (1 h interval), 24 h, and 72 h after NaCl addition. To interpret the results, we first consider DNA-**6**. Fig. 3a–e show that DNA-**6** emission spectrum evolves over time for specific concentrations of NaCl.

Fig. 4 summarizes percent intensity change of the peak that increased most significantly with NaCl addition for each DNA strand. DNA-**6** exhibits the most dramatic intensity increase with NaCl, up to 30-fold for 1000 μM NaCl at 72 h (Fig. 4f). For DNA-**1**, **2**, and **3**, which form both visible and NIR species, only visible species increase in intensity with NaCl addition (Fig. 4a–c), while associated NIR-emissive species either undergo smaller intensity increases or are unstable in NaCl (Fig. S7, ESI†). Specific emission spectral changes in the presence of NaCl vary widely among emitters and may depend sensitively on specific nanocluster structure. For example, DNA-**4** and **5** form emitters that brighten at 250 μM NaCl, whereas visible species from DNA-**1**, **2** and **3** require 750 or 1000 μM NaCl concentrations for significant increase. These results support that variations in residual chloride in commercial oligomers could contribute to discrepancies between Ag$_N$-DNA batches, possibly favoring formation of visible Ag$_N$-DNAs over NIR Ag$_N$-DNAs. Ongoing research is focused on the chemical synthesis process for Ag$_N$-DNAs with chlorido ligands, which is beyond the scope of this study.

We hypothesize that changes in nucleobase pK_a with temperature and pH are partly responsible for observed changes in

Fig. 3 Emission spectra for DNA-**6** at 0 to 6, 24, and 72 h (legend) (a) without NaCl (0 μM) and after addition of NaCl at (b) 250 μM, (c) 500 μM, (d) 720 μM, and (e) 1000 μM.
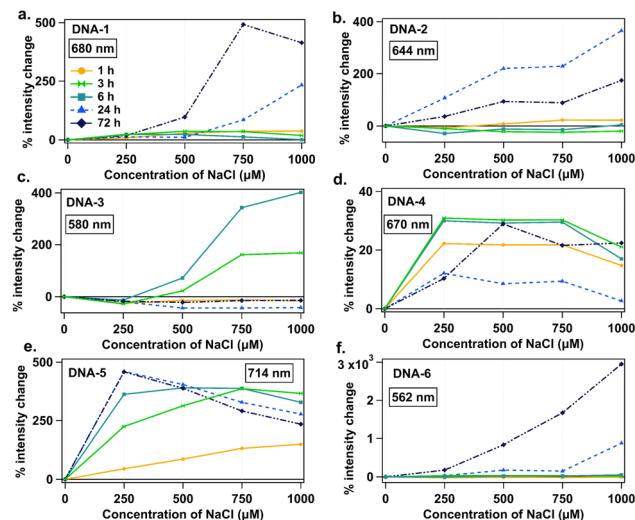
Fig. 4 Percent intensity change as a function of NaCl concentration for (a) DNA-**1**, (b) DNA-**2**, (c) DNA-**3**, (d) DNA-**4**, and (e) DNA-**5**, and (f) DNA-**6**, specifically for the emission peak that increases the most with NaCl addition. Legend represents time points of 1 (yellow circles), 3 (green double triangles), 6 (teal squares), 24 (light blue triangles), and 72 hours (navy diamonds). Fig. S8 (ESI†) also shows data for 2, 4, and 5 hours.

formation of NIR Ag_N-DNAs between microwell plate and single tube synthesis, with additional effects from variations in residual salts. Since changes in nucleobase pK_a with temperature and pH depend on oligomer length and neighboring nucleobases,[33] these effects will be sequence specific and may be complex. Sensitivity of Ag_N-DNAs to pH and halide ions could be exploited for novel biocompatible sensors. Future studies may determine why NIR-emissive products tend to favor basic pH and elevated temperature.

In summary, we showed how storage temperature, solution pH, and small amounts of NaCl influence chemical yield of visible and NIR-emissive Ag_N-DNAs. Increased storage temperature of Ag_N-DNAs post-reduction can significantly increase emission intensity of far red and NIR Ag_N-DNAs, and in some cases is crucial to form measurable amounts of NIR Ag_N-DNAs. Basic pH promotes formation of NIR DNAs, whereas near-neutral pH favors red and far-red Ag_N-DNAs. Lastly, NaCl can significantly increase brightness of red and far-red Ag_N-DNA species. The synthesis strategies presented here are critical for the study of NIR-emissive Ag_N-DNAs and may expedite development of these fluorophores for NIR fluorescence bioimaging. Researchers using recently reported libraries of DNA template sequences for NIR Ag_N-DNAs[12,16] should employ these synthesis methods, rather than conventional Ag_N-DNA synthesis methods that often favor smaller, visibly emissive Ag_N-DNAs.

Conflicts of interest

There are no conflicts to declare.

Notes and references

1 Y. Chen, M. L. Phipps, J. H. Werner, S. Chakraborty and J. S. Martinez, *Acc. Chem. Res.*, 2018, **51**, 2756–2763.
2 R. Guha and S. M. Copp, in *Modern Avenues in Metal-Nucleic Acid Chemistry*, ed. J. Müller and B. Lippert, CRC Press, 2023, ch. 12, pp. 291–342.
3 A. Gonzàlez-Rosell, C. Cerretani, P. Mastracco, T. Vosch and S. M. Copp, *Nanoscale Adv.*, 2021, **3**, 1230–1260.
4 R. Guha, A. Gonzàlez-Rosell, M. Rafik, N. Arevalos, B. Katz and S. Copp, *ChemRxiv*, 2023, DOI: **10.26434/chemrxiv-2023-hftx9**.
5 S. M. Copp, D. Schultz, S. Swasey, J. Pavlovich, M. Debord, A. Chiu, K. Olsson and E. Gwinn, *J. Phys. Chem. Lett.*, 2014, **5**, 959–963.
6 E. G. Gwinn, P. O'Neill, A. J. Guerrero, D. Bouwmeester and D. K. Fygenson, *Adv. Mater.*, 2008, **20**, 279–283.
7 S. A. Bogh, M. R. Carro-Temboury, C. Cerretani, S. M. Swasey, S. M. Copp, E. G. Gwinn and T. Vosch, *Methods Appl. Fluoresc.*, 2018, **6**, 024004.
8 V. A. Neacşu, C. Cerretani, M. B. Liisberg, S. M. Swasey, E. G. Gwinn, S. M. Copp and T. Vosch, *Chem. Commun.*, 2020, **56**, 6384–6387.
9 J. Yu, S. Choi, C. I. Richards, Y. Antoku and R. M. Dickson, *Photochem. Photobiol.*, 2008, **84**, 1435–1439.
10 J. Yu, S. Choi and R. M. Dickson, *Angew. Chem., Int. Ed.*, 2009, **48**, 318–320.
11 S. Y. New, S. T. Lee and X. D. Su, *Nanoscale*, 2016, **8**, 17729–17746.
12 P. Mastracco, A. Gonzàlez-Rosell, J. Evans, P. Bogdanov and S. M. Copp, *ACS Nano*, 2022, **16**, 16322–16331.
13 S. M. Copp, P. Bogdanov, M. Debord, A. Singh and E. Gwinn, *Adv. Mater.*, 2016, **28**, 3043.
14 S. M. Copp, A. Gorovits, S. M. Swasey, S. Gudibandi, P. Bogdanov and E. G. Gwinn, *ACS Nano*, 2018, **12**, 8240–8247.
15 S. M. Copp, S. M. Swasey, A. Gorovits, P. Bogdanov and E. G. Gwinn, *Chem. Mater.*, 2020, **32**, 430–437.
16 S. M. Swasey, S. M. Copp, H. C. Nicholson, A. Gorovits, P. Bogdanov and E. G. Gwinn, *Nanoscale*, 2018, **10**, 19701–19705.
17 B. Sengupta, C. M. Ritchie, J. G. Buckman, K. R. Johnsen, P. M. Goodwin and J. T. Petty, *J. Phys. Chem. C*, 2008, **112**, 18776–18782.
18 G. Hong, A. L. Antaris and H. Dai, *Nat. Biomed. Eng.*, 2017, **1**, 0010.
19 A. Gonzàlez-Rosell, R. Guha, C. Cerretani, V. Rück, M. B. Liisberg, B. B. Katz, T. Vosch and S. M. Copp, *J. Phys. Chem. Lett.*, 2022, **13**, 8305–8311.
20 C. Cerretani, J. Kondo and T. Vosch, *RSC Adv.*, 2020, **10**, 23854–23860.
21 C. Cerretani, J. Kondo and T. Vosch, *CrystEngComm*, 2020, **22**, 8136–8141.
22 M. B. Liisberg, Z. Shakeri Kardar, S. M. Copp, C. Cerretani and T. Vosch, *J. Phys. Chem. Lett.*, 2021, **12**, 1150–1154.
23 C. Cerretani, H. Kanazawa, T. Vosch and J. Kondo, *Angew. Chem., Int. Ed.*, 2019, **58**, 17153–17157.
24 A. Gonzàlez-Rosell, S. Malola, R. Guha, N. R. Arevalos, M. F. Matus, M. E. Goulet, E. Haapaniemi, B. B. Katz, T. Vosch, J. Kondo, H. Häkkinen and S. M. Copp, *J. Am. Chem. Soc.*, 2023, **145**, 10721–10729.
25 J. T. Petty, C. Fan, S. P. Story, B. Sengupta, A. S. Iyer, Z. Prudowsky and R. M. Dickson, *J. Phys. Chem. Lett.*, 2010, **1**, 2524–2529.
26 J. T. Petty, C. Fan, S. P. Story, B. Sengupta, M. Sartin, J. C. Hsiang, J. W. Perry and R. M. Dickson, *J. Phys. Chem. B*, 2011, **115**, 7996–8003.
27 J. Müller, *Coord. Chem. Rev.*, 2019, **393**, 37–47.
28 S. Naskar, R. Guha and J. Müller, *Angew. Chem., Int. Ed.*, 2020, **59**, 1397–1406.
29 J. Kondo, Y. Tada, T. Dairaku, Y. Hattori, H. Saneyoshi, A. Ono and Y. Tanaka, *Nat. Chem.*, 2017, **9**, 956–960.
30 S. M. Swasey, N. Karimova, C. M. Aikens, D. E. Schultz, A. J. Simon and E. G. Gwinn, *ACS Nano*, 2014, **8**, 6883–6892.
31 C. Cerretani, M. R. Carro-Temboury, S. Krause, S. A. Bogh and T. Vosch, *Chem. Commun.*, 2017, **53**, 12556–12559.
32 S. M. Copp and A. Gonzàlez-Rosell, *Nanoscale*, 2021, **13**, 4602–4613.
33 J. C. González-Olvera, J. Martínez-Reyes, E. González-Jasso and R. C. Pless, *Biophys. Chem.*, 2015, **206**, 58–65.
34 J. D. Lee, J. Cang, Y.-C. Chen, W.-Y. Chen, C.-M. Ou and H.-T. Chang, *Biosens. Bioelectron.*, 2014, **58**, 266–271.
35 M. Gambucci, C. Cerretani, L. Latterini and T. Vosch, *Methods Appl. Fluoresc.*, 2019, **8**, 014005.